Biophysical Chemistry 203–204 (2015) 1–11

Contents lists available at ScienceDirect

Biophysical Chemistry

journal homepage: http://www.elsevier.com/locate/biophyschem

# Molecular dynamics of Kv1.3 ion channel and structural basis of its inhibition by scorpion toxin-OSK1 derivatives

Rajabrata Bhuyan [a], Alpana Seal [b,*]

[a] BIF Centre, Department of Biochemistry & Biophysics, University of Kalyani, Kalyani, Nadia, West Bengal PIN – 741235, India
[b] Department of Biochemistry & Biophysics, University of Kalyani, Kalyani, Nadia, West Bengal PIN – 741235, India

## HIGHLIGHTS

- Kv1.3 ion channel in closed conformation is more preserved than open state.
- It followed the same paddle model of channel gating for channel activation.
- Large structural variations are observed in OSK1 derivatives after mutation.
- Any mutation of OSK1 doesn't have direct role in the Kv1.3 inhibition.
- Residues responsible for specific interaction with OSK1 in Kv1.3 are identified.

## GRAPHICAL ABSTRACT

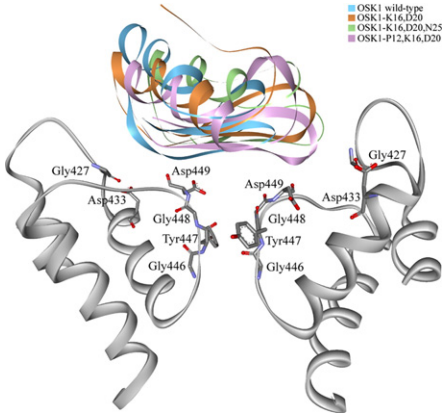


## ARTICLE INFO

*Article history:*
Received 22 January 2015
Received in revised form 22 April 2015
Accepted 22 April 2015
Available online 29 April 2015

*Keywords:*
Voltage-gated
$K^+$ channel
*Shaker*-type
Inhibition
OSK1
MD simulation

## ABSTRACT

Kv1.3 is one of the widely distributed *Shaker* type voltage gated potassium channel which performs the outward flow of $K^+$ ions in excitable cells. In immunological synapse, Kv1.3 plays a pivotal role in antigen dependent activation and proliferation of lymphocytes along with the $K_{Ca}3.1$. The up-regulation of Kv1.3 leads to several T-cell-mediated autoimmune diseases, hence considered as an attractive pharmacological drug target. Here, we have employed molecular modeling, docking and simulation techniques to examine the dynamical properties of Kv1.3 in both open and closed state conformation embedded in DPPC membrane as well as its modes of inhibition against the popularly known scorpion venom OSK1 and its three mutant analogues. The Kv1.3 in open conformation took comparatively more time to get stabilized than the closed state. Both conformations ascertain their stability and the transition between closed to active states is more consistent with the paddle model of channel gating. The binding modes of channel–toxin complexes are well established by identifying strongly interacting amino acids lining at their polar surfaces. Our findings suggest that, two mutant derivatives OSK1-K16,D20 & OSK1-P12,K16,D20 have increased inhibitory potency against Kv1.3. We also pointed out some particular residues responsible for binding of OSK1 with Kv1.3 over other *Shaker*-type ion channels. We believe that the insights came from Kv1.3–OSK1 interaction will be valuable in pharmacological studies for strategic development of both potent and selective therapeutic drugs against T-cell-mediated autoimmune diseases.



* Corresponding author. Tel.: +91 33 2582 3405.
*E-mail addresses:* rajabrata001@gmail.com (R. Bhuyan), aseal@klyuniv.ac.in (A. Seal).

http://dx.doi.org/10.1016/j.bpc.2015.04.004
0301-4622/

## 1. Introduction

Kv1.3 encoded by *KCNA3* gene is one of the mammalian voltage-gated *Shaker*-type potassium channels of delayed rectifier group, which plays critical role in generating the action potential in both excitable and non-excitable cells of organs like brain, lung, kidney, and olfactory bulbs [1–6]. The usual architecture of the Kv1 channel family is tetrameric, typically consisting of six transmembrane helical segments (S1–S6) in each subunit. The first four anti-parallel helical segments (S1–S4) at the periphery of the channel core are known as voltage sensing domains (VSDs), located inside the lipid environment and the last two helices S5 & S6 form the ion selective pore [7–10]. Upon membrane depolarization, movements of VSDs in each subunit lead the channel to opt an ion conducting open conformation, whereas it maintains its resting state during membrane hyperpolarization [11–15]. In recent years, many crystal structures of eukaryotic *Shaker*-type potassium channel of family 2 (Kv1.2) in open conformation has been deposited in RCSB [16–20]. Due to the unavailability of its resting state conformation, computational techniques are employed to translate the results of various wet lab experiments into structural insights [21–24]. Rather than the conserved transmembrane helices, members of Kv1 channel show high level of sequence variability in their extracellular/intracellular loops. So in this work, we have tried to address the independent structural activities of kv1.3 in both open/closed conformations in depolarized potential.

In effector memory T cells ($T_{EM}$), Kv1.3 channel assists the T lymphocyte activation along with the $K_{Ca}3.1$ by means of the potassium efflux as well as the calcium influx to counterbalance the ion concentration of the cell [25,26]. During the activation of $T_{EM}$ cells, expression of the Kv1.3 channel is up-regulated significantly, ranging normally from 300 molecules to ~1500–2000 molecules per cell [27]. These differential expressions of Kv1.3 lead to many T-cell-mediated autoimmune diseases such as multiple sclerosis, type 1 diabetes, and rheumatoid arthritis [28,29]. Consequently, for the preferential inhibition of $T_{EM}$ cells, Kv1.3 channel has been considered as suitable target [30–32]. During past three decades, many selective blockers of Kv1.3 have been identified and among them, peptide inhibitor ShK-186 has been proved to block the proliferation & migration of $T_{EM}$ cells. Other than ShK-186, many other small compounds and polypeptides such as ChTX, MTX and OSK1 that occlude the Kv1.3 channel effectively have also been reported [28,33–35]. These peptide blockers are mostly the toxins from venomous animals having affinities towards Kv1.3 as well as for Kv1.1 and/or Kv1.2 channel. But the discovery of more potent and selective Kv1.3 channel inhibitors is still a greatly needed task to strengthen the therapeutic approach. Thus, rather than searching for a new inhibitor, we concentrated on the well studied OSK1 and their mutant analogous to understand the structural mechanism of their specific interaction with Kv1.3.

OSK1 or alpha-KTx 3.7 is a venom toxin from central Asian scorpion *Orthochirus scrobiculosus* belonging to a structural class referred to as α-KTx3 [36]. It contains 38 amino acid residues cross-linked by three disulfide bridges in a conventional fashion (C1–C4, C2–C5 and C3–C6) [37]. The NMR structure of OSK1 (PDB ID: 1SCO) shows that the peptide adopts the popular α/β scaffold conformation which is very common among most characterized scorpion venoms [36]. Pharmacological studies of natural OSK1 reveal that, it blocks the *Shaker*-type Kv1.1, Kv1.2 & Kv1.3 channels potently with $IC_{50}$ values of 0.6, 5.4 and 0.014 nM respectively [38,39]. On the other hand, a synthetic form of OSK1 (OSK1-K16,D20) has been established to be the most potent and selective scorpion toxin inhibitor of Kv1.3, which blocks the channel with an $IC_{50}$ of 3 pM and shows more than 300-fold selectivity over other potassium channels [39]. Several other analogues of OSK1 have been discovered so far with selective mutations and modified inhibitory activities against Kv1.3. However, the structural adaptations of these mutant derivatives are unknown and their interaction with Kv1.3 is still not studied properly. Hence, we modeled the 3D structure of these OSK1 analogues and predicted their equilibrated conformation using MD simulation. Overall, we have demonstrated the conformational dynamics of Kv1.3 channel in both open & closed states embedded in DPPC membrane and verified its inhibition by OSK1 along with its three mutant derivatives. Here we will provide some useful information and clues about the biophysical behavior of human Kv1.3 and its specific interaction with OSK1.

## 2. Materials & methods

### 2.1. Generating the 3D models of Kv1.3 & OSK1

Amino acid sequence of human Kv1.3 was downloaded from UniProt protein database (UniProt ID: P22001). All the members of *Shaker*-type Kv channel possess conserved amino acids in transmembrane helices, whereas sequence variability is found only at the intra & extracellular loops connecting those helices. Kv1.3 is of 575 amino acids long with an extended N-terminal region and shares 72.67% sequence identity with its native Kv1.2, which has the only full length crystal structure in open state of this family. But due to the high dynamics and/or static disordering, ~37% of this structure was incomplete in its intracellular or extracellular loop regions [16]. So the atomic models of Kv1.2 in open and closed state conformation proposed by Pathak et al. derived by the Rosetta-Membrane structure prediction program were taken as the template to build the homology model of human Kv1.3 [21]. The stereochemistry of both the models was verified by several web tools through Structural Analysis and Verification Server (SAVES) at http://nihserver.mbi.ucla.edu/SAVES/. All types of sequence analysis were performed using ClustalX sequence analysis program [40].

The atomic coordinates of OSK1 (PDB ID: 1SCO) [36] was obtained from the Protein Data Bank. Three more derivatives of OSK1 such as OSK1-K16,D20, OSK1-K16,D20,N25 and OSK1-P12,K16,D20 were generated. Comparative modeling program MODELLER of DISCOVERY STUDIO 2.5 was used to predict the 3D structure of Kv1.3 in both open and closed states as well as of OSK1 analogues [41]. All the generated models were refined via loop optimization and on the basis of DOPE score, the best models were chosen.

### 2.2. MD simulation protocols

In this work, all the simulations were performed using GROMACS 4.6.3 packages [42] in a 32 node Lenovo D30 workstation. Every type of calculations and analyses were carried out by the GROMACS suite of tools along with a secondary structure recognition algorithm (DSSP) [43]. Microsoft Excel program was used for preparation of the graph and for structure visualization, DS Visualizer and PyMOL were employed [44].

### 2.3. MD simulation of Kv1.3

The protocol described in our previous work was followed for MD simulation of Kv1.3 both in open and closed states [45]. Both the systems were comprised of Kv1.3 tetrameric conformation of 1556 amino acids embedded in a dipalmitoylphosphatidylcholine (DPPC) bilayer with 499 and 500 DPPC molecules of each for open and closed systems respectively. After solvation and system neutralization by 100 mM KCl, the total numbers of atom reached in both the systems to 216,434 and 201,491, respectively for open and closed conformations. For stabilization of the pore, 3 K ions were put near the selectivity filter.

### 2.4. MD simulation of OSK1

Additional simulations were performed to equilibrate OSK1 toxin in wild-type and three mutated forms. So in total, four systems of OSK1

were prepared and subjected to simulation using Charmm27 (Chemistry at Harvard Macromolecular Mechanics) all atom force field [46]. The peptides were protonated and solvated by explicit SPC/E water model in cubic boxes with minimum edge distance of 10 Å [47]. A salt concentration of 0.10 M NaCl was maintained to achieve the system electrically neutral. Then the systems were subjected for energy minimization process using steepest descent integrator followed by temperature (NVT) and pressure (NPT) equilibration. An initial 100 ps NVT ensemble was performed with velocity rescale thermostat [48] to stabilize the temperature of the system at 323 K by restraining all of the backbone protein atoms to reorient water around exposed proteins. The systems were then subjected for NPT equilibrium of 100 ps, during which all the restraints were removed. During NPT, velocity rescale thermostat and Parrinello–Rahman barostat algorithm [49] were implemented respectively for temperature and pressure coupling. Production run was carried out for 50 ns as the continuation of NPT under periodic boundary conditions where the protein and solvent (waters and ions) were separately coupled. The system temperature was achieved using the Velocity rescale at 323 K, with a coupling time constant ($\tau T$) of 0.8 ps and the pressures were coupled by isotropic Parrinello–Rahman barostat at 1 bar, via a coupling constant of $\tau P = 2$ ps and compressibility at $4.5 \times 10^{-5}$ $bar^{-1}$. Cutoff distances for the calculation of short-range coulombic and van der Waals interaction were set to 12 Å with a Fourier grid spacing distance of 1.6 Å and the long range electrostatic interactions were calculated according to the Particle Mesh Ewald (PME) algorithm [50]. All bond lengths were constrained using the linear constraint solver (LINCS) algorithm [51].

### 2.5. Modeling Kv1.3 and OSK1 complexes and their simulation

The truncated version of Kv1.3 channel including all the transmembrane segments (AA no. 220–491) along with the equilibrated and minimized average structures of OSK1 were taken subsequently to build Kv1.3–OSK1 complexes using rigid body molecular docking program, ZDOCK of Discovery Studio 2.5 [52]. As per the mutagenic studies, amino acids present in the extracellular part and selectivity filter of Kv1.3 were restricted for peptide inhibitory sites where, the OSK1s were allowed to interact free. For each case, 2000 channel–toxin bound state conformations were generated and out of them, we selected the most consistent complex relating with the experimental findings [53,54]. There was an account of less than 2% of complexes where lysine residue at position 27 of the toxin was docked into the channel selectivity filter and we chose the best complexes based on top ranked score, satisfying the above criteria of potassium channel–toxin interaction. The selected complexes predicted by the rigid body docking were an inadequate representation of the bound states. Hence MD simulations were performed to study their interaction dynamics. Four simulation boxes were prepared again for the Kv1.3–OSK1 complexes surrounded in a DPPC membrane environment following the previously described simulation procedure. At constant pressure, time evolution of all the system dimensions was considered to access their equilibrium. Again to calculate the binding free energies and the difference in binding site solvent accessible surface area, simulations of independent OSK1 and its derivatives were executed separately. The binding free energy differences were carried out by linear interaction energy (LIE) based solvation method [55,56]. LIE approach depends on the atomic charge model used to delineate the coulomb interaction between the ligand and its environment. It estimates the binding affinities from the van der Waals and electrostatic interaction energies for the ligand in water and the ligand in complex with solvated protein, which helps to understand detailed interactions between receptor and ligand.

The LIE equation is given as:

$$G_{binding} = \alpha\Delta E_{vdw} + \beta\Delta E_{elec} + \gamma = \alpha(E_{B\_vdw} - E_{F\_vdw}) + \beta(E_{B_{elec}} - E_{F\_elec}) + \gamma.$$

The $\Delta$ term indicates the difference in energy of ligand in free (EFree) and bound (EBound) states. The $\alpha$, $\beta$ and $\gamma$ are LIE empirical parameters or scaling factors, calculated from experimentally estimated binding affinities. In our studies, the default values of 0.18 and 0.50 are taken as the scaling factors respectively for $\alpha$, $\beta$. Another component $\gamma$ is an additional constant necessarily considered for reasonable binding free energy predictions, was set to zero.

## 3. Results & discussions

### 3.1. Stability of Kv1.3 channel in open and closed conformation

The equilibrated conditions of both systems were established in terms of their root-mean square deviations (RMSD), residue wise fluctuations and intermolecular interactions during the 50 ns time span of simulation. Unlike the other *Shaker*-type Kv channels, the Kv1.3 exhibits fairly "rapid inactivation" property irrespective of amino acid similarities with "delayed rectifier" group and possess a bit close resemblance with "A-type potassium channel" family [57,58]. This characteristic was constantly viewed in our study, where the closed conformation of Kv1.3 channel showed more stability in comparison with the other *Shaker*-type channels, such as Kv1.1 or Kv1.2. In Kv1.3 open state model, RMSD of transmembrane helices increases rapidly during the first 7 ns, and reaches to equilibrium with a maximum deviation of ~5 Å from its initial conformation after 40 ns of simulation. Whereas in case of closed state, it attains its equilibrium very quickly (just after 7 ns of simulation) and gets more time for relaxation inside the lipid bilayer system (Fig. 1A and B). A gradual fluctuation in the RMSD of independent voltage sensor S4 helix is observed because of the movement of charged amino acids, it carries through the membrane electric field. The S4 helix in open model is the prime contributor of overall channel RMSD, which varies in an average deviation of 3.5–4.4 Å. But in closed conformation, it remains around of 3 Å which is easily viewed to be more stable than the open state. Unlike the S4 helix, the central pore forming residues (TVGYGD, 444–449) shared by all the four chains are said to be more rigid than the other parts of protein. For the first few ns, there is nearly a rough deviation of 2 Å and it continues till the end in open state. However, it vacillates a bit more between 2.7–3.2 Å in closed conformation throughout the simulation (Fig. 1A and B). The relative stability attained by pore of the open conformation is more possibly due to its favorable interaction with $K^+$ ions. However, the overall structural conformation of closed model is comparatively more preserved (Fig. 1C).

Simultaneously we calculated the average Cα root-mean-square fluctuations (RMSFs) of all the identical chains of both the models in order to identify the most fluctuating regions of different domains as a function of their residue number (Fig. 1C). From the RMSF data, it is clear that all four subunits of each model exhibit virtually almost equal patterns. The most prominent peaks are found at the cytoplasmic parts, and in the extracellular and intracellular loops compared to the transmembrane helices. Overall Kv1.3 in open model is more mobile than the closed state conformation. The ion selective pore in both the cases shows remarkable stability with an average fluctuation of 1.57 & 1.12 Å in contrast with the voltage sensor S4 helix, which is at 1.81 & 1.71 Å for open and closed model respectively. However, the "helix-turn-helix" conformation near the C-terminal of S3 and the N-terminal portion of S4 (VS paddle) [22,70], which is necessary in usual channel gating has been found fluctuating amazingly in open state conformation than the closed one. This data is also consistent with their DSSP secondary structure plots. The overall secondary structure pattern of Kv1.3 in both the open & closed state is almost preserved (Fig. S1 of Supplementary data), except the solvent-exposed loops on the extracellular and intracellular surfaces, which do not have any proper secondary structure. According to studies, the S1–S2 surface loop of Kv1.3 bears a glycosylation site, necessary for several biological activities of the channel [59,60]. This linker in Kv1.3 contains 41 amino acid

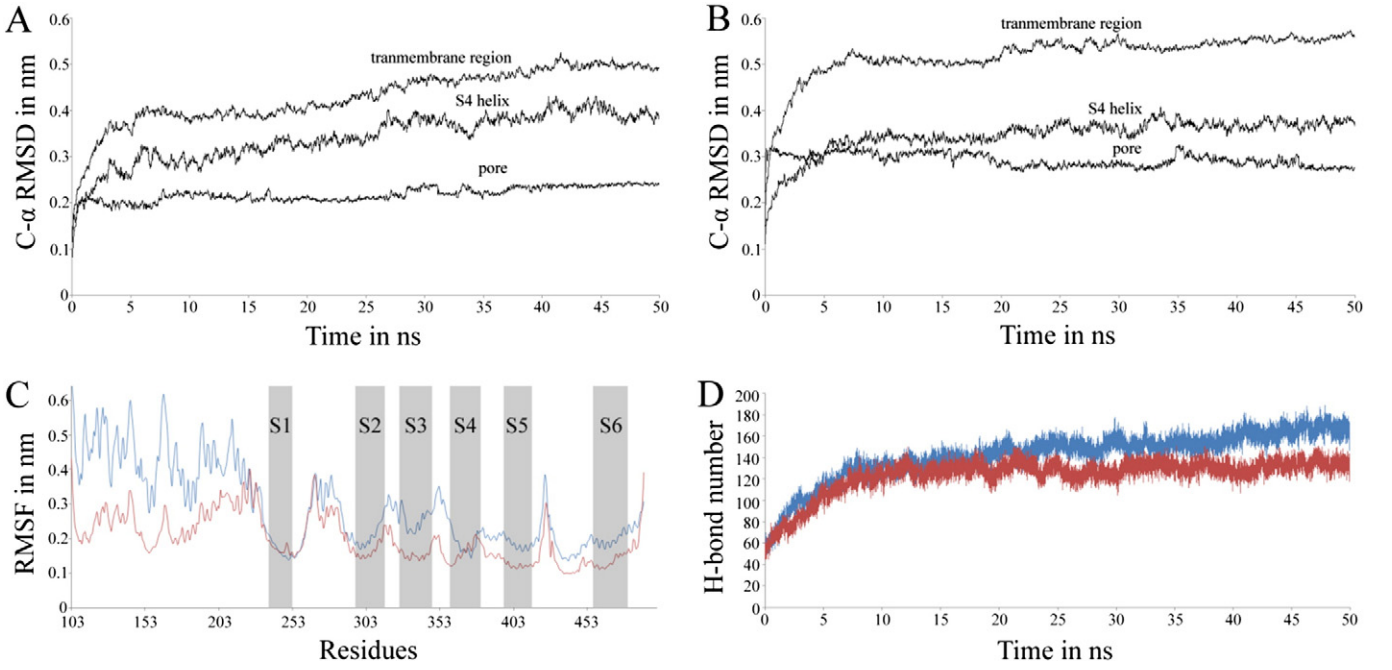


**Fig. 1.** Cα atomic RMSD of transmembrane segments, voltage sensor S4 helix and ion selective pore in open model (A) & (B) closed model. (C) Comparison of Cα RMS fluctuations between open (blue) & closed model (red) as a function of residue number. (D) Number of hydrogen bonds between protein and lipid throughout the simulation period, referring blue for open & red for closed state conformation.

residues, which is a bit more extended in comparison to other *Shaker*-type channels such as Kv1.1 & Kv1.2 and remains almost exposed to the extracellular solution (Fig. S2 of Supplementary data). In Kv1.3 open state conformation, the region at this particular linker is comparatively more mobile than closed model. The previous simulations on other *Shaker*-type Kv channel state that the S1–S2 linker in active state has to be more excited than inactive/closed conformation and supposed to have mostly a random coil, lacking helical structure [61,62]. It is also confirmed from the studies of Villalba-Galea et al. that a small region of this linker should turn into α-helical, which has a little effect on its voltage-dependent opening [63]. The same feature is observed and well maintained in three out of four chains of Kv1.3 open model throughout simulation. But in Kv1.3 closed model, no particular secondary structure is seen in this region.

Traditionally the cytoplasmic end of S4 helix is intended to adopt a $3_{10}$ helical conformation while switching from inactive to open active form of the channel [64], which is also supported by the two X-ray structures in open state and our previous simulation on Kv1.1 [10,65,45]. But here in case of Kv1.3, rather than forming a $3_{10}$ helix, the lower end of S4 transforms into a turn like conformation in open model due to the orientation of gating arginines towards the water-filled crevice formed by VSDs. However, no such modification is observed in closed state.

The solvent-exposed S4–S5 linker holds a clean helical structure in both the models throughout the simulation (Fig. S1). This linker is a short amphipathic α-helix that rests parallel to membrane. Usually, the stability of this linker is a consequence of its amino acid composition where the residues facing the lipid are hydrophobic in nature and the alternate hydrophilic residues remain in contact with water [16]. The conformational changes in VSDs affect the channel gating via S4–S5 linker as a result of opening or closing of ion conduction pathway. Here, mobility of this linker is visibly marked in RMSF plot, relating to the instance of gating charge transfer of Kv1.3 channel. The transmembrane structure near the pore region remains almost distinctly α-helical in both the states of Kv1.3 channel.

We also considered the change in potential energy, number of hydrogen bond interactions between the protein and the lipid bilayer in both the models as a function of their stability. We observed the potential energies of both systems are stabilized just after few ns of simulation. The H-bond numbers between protein and lipids take more than 20 ns to reach the equilibrium, resulting to 20–30 H-bonds between both the models starting from their initial conformation (Fig. 1D).

### 3.2. Movement of S4 helix and stabilization

#### 3.2.1. Salt bridges within the voltage sensor

In response to transmembrane potential, all the subunits of both the models lost their symmetry just after few pico seconds of simulation by the movement of VSDs (S1–S4). The S4 helix was the most affected one where voltage dependant charge carrying residues are present in every third position along the helix. Six gating charged residues including five arginines and one lysine confined in S4 helix are R364, R367, R370, R373, K376 & R379, also termed as R1, R2, R3, R4, K5 & R6 respectively. We recorded the pattern of their H-bond formation and salt bridge interactions in both the models as a function of their conformational changes made by channel upon depolarization.

Mostly in open state, the initial charged residues of S4 (R1 & R2) are found to be positioned near the extracellular leaflet of lipid bilayer, interacting through numerous H-bonds and stable salt bridges with the membrane. But in case of closed one, C-terminal end of S4 (R4, K5 & R6) is pushed deeply towards the intracellular region, bound to the lipid. R2 & R3 of open model form two stable salt bridges with negatively charged amino acids E254 & E258 at the C-terminal end of S1 helix, and also get close with D261 & E262 for a while over the length of the simulation. A salt bridge between R4 & E254 remains stable in three out of four subunits. K5 contributes long lived interaction with D332 of S3 helix and transient interaction with R313 of S2. The initial salt bridge distance between R6 & D332 increases and R313 provides stable interaction to R6. Two other negatively charged amino acids E299 & E309 of S2 (popularly known as E1 & E2) participate in interaction with R4 & K5 observed in all chains of Kv1.3 open model.

On the other hand in closed state conformation, R1 & R2 were detached from external lipid layer and normally surrounded by the VSDs. R1 maintains two stable salt bridges with E254 & E258 and the initial interaction between R1 & E1 disappeared after few ns of

simulation. Similarly, the R2 is associated with E1 & D332 by salt bridge, noticed in every segment. The R3 & R4 are comparatively more exposed towards the intracellular region as well as interact with E2 & D332 in an alternative manner. While K5 & K6 are solely located in the DPPC membrane and don't form any contact with the other VSD residues.

Comparison of salt bridge formation by these S4 key residues of Kv1.1, Kv1.2 and Kv1.3 are given in Table SI of the Supplementary data. It reveals that the positions of these residues took more time to get stable than the other two *Shaker*-type channel, as most of the salt bridges persist for long time before they get detached for a new bridge during the movement of S4 helix (Table SI of Supplementary data).

### 3.2.2. Drift of the S4 segment

The movement of voltage sensor domain affects the channel activity; hence influences the gating mechanisms of this type of ion channel. We calculated the displacement of those charge carrying residues of S4 helix to interpret their gating motions in accordance with their conformational stability. The vertical displacements of C-α atom of these key residues along the z-axis, parallel to the membrane normal (taking average of four chains) are traced and shown in Fig. 2. In case of the open state conformation, they all shift almost in a same manner, travel upward in the membrane core from their initial positions except the R1, which tends to cling at its original place (Fig. 2A). These residues in closed model move rapidly up in the bilayer within first 5 ns of simulation and changed their direction in reverse towards the intracellular region, where it can induce several stable electrostatic interaction and H-bonds with the membrane (Fig. 2B). The initial positional difference of residues R1, R2, R3, R4, K5 and R6 from closed to open state were 0.82 1.027 1.12 0.77 0.23 & −0.042 nm respectively and reached to equilibrium at 0.402, 0.727, 0.806, 0.530, 0.071 & −0.003 after 10 ns of simulation. That shows 6–8 Å of overall deviation in S4 is achieved from closed to open state transition (Fig. 2C) which is in agreement with the average vertical movement of S4 residues between close and open state calculated from voltage-clamp fluorometry study [21].

The tilt angle (between the S4 helix and membrane plane) of Kv1.3 open model shows a rapid fluctuation and stabilizes with an average value of 143° after 10 ns of simulation. However, no such variation is observed in closed state conformation. The change in tilt from closed to open state conformation balances at 17°–23° after 23 ns of simulation in contrast to the initial value of 11° (Fig. 2D).

### 3.3. Gating mechanisms of Kv1.3 channel

The gating mechanism of *Shaker*-type ion channel has been described via transporter model, helical screw model and paddle model with respect to the movement of charge-carrying residues of S4 segment in the surrounding environment [65]. Usually in case of helical screw or sliding helix models of voltage gating, the S4 helix rotates and translates along its axis from intracellular to extracellular region inside the protein environment [66,67]. But in paddle model of channel gating, C-terminal end of S3 together with the N-terminal part of S4 helix (upper portion) form a paddle like conformation, which locates deep in the membrane at resting state and upon depolarization, it translates at a displacement of 15–20 Å across the membrane axis along with a large rotation [22]. It's evident that, S4 helix should be connected to the lipids by both ends and the conformational changes required to attain the channel's open activated state is achieved by an upward movement of the helix [68,69]. It is also clear from the crystal structure of the Kv1.2 channel in open conformation that, 20–25% of S4 helix was partly exposed to lipids by both ends and the channel follows the paddle model of channel gating to get activated [15,68]. This has been clarified by the salt bridge interaction and drift of S4 helix among the VSDs from our studies. Interaction pattern of charged residues taken from the time evolution of the systems confirm that, the first three arginines (R1, R2 & R3) of open model rapidly adopt a location, exposed to the upper lipid environment at equilibrium. The orientation of these arginine side chains have been affected mostly due to the lack of membrane phosphate head groups in the protein environment. Similarly, the downstream residues K5 & R6 are found to lose their initial interactions from negatively charged residues of S2 & S3 helices and also from the intracellular membrane layer. In closed state of conformation, the C-terminal end of S4 (R4, K5 & R6) continued to exist near intracellular region close to the lipid where the arginines R1 & R2 remain surrounded by the other VSDs and far away from lipid.

The vertical fluctuations (along the z axis) of these charged residues of S4 helix monitored from the trajectories show a possible 2 Å upward displacement in open model at equilibrium (Fig. 2A). However, due to the extreme flexibility of VSDs, estimating the vertical translation of S4 helix always face some uncertainty. Even in two crystal structure of Kv1.2, the vertical position of R1 differs by 2.6 Å [16,17]. From the short period of our simulation studies, both the upward and downward movement of S4 have been observed in open & closed states of

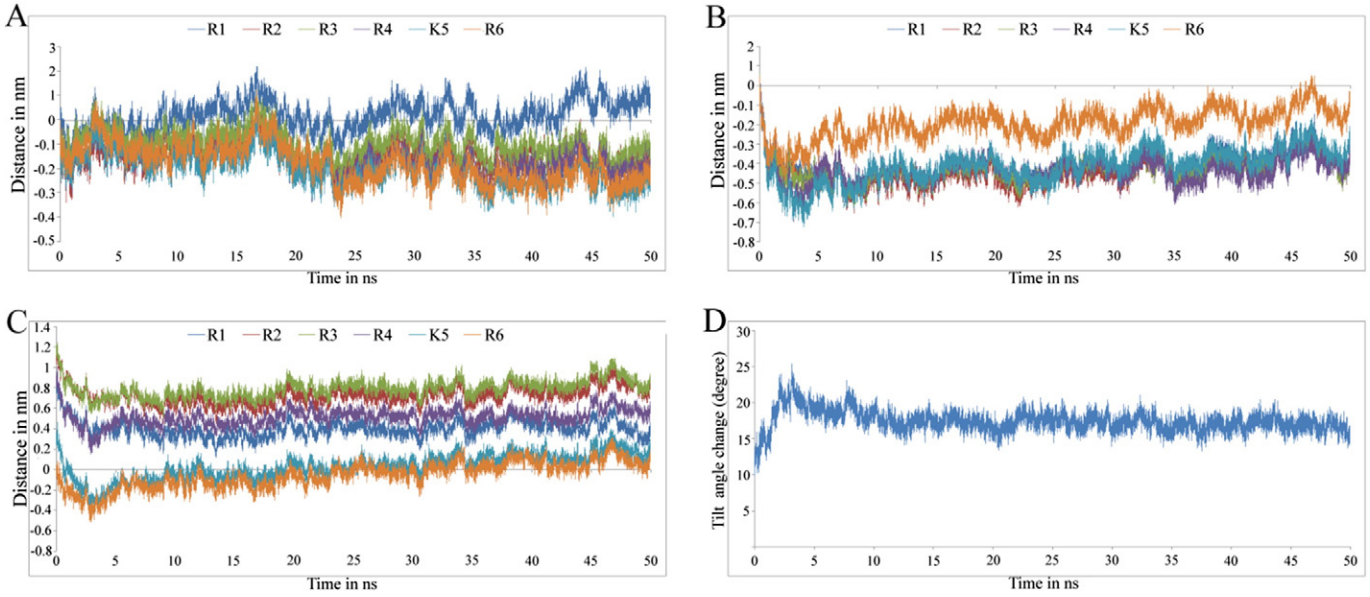


**Fig. 2.** Vertical displacement of charged residues in S4 helix in (A) open & (B) closed models, (C) from closed to open state with reference to time. (D) The change in tilt angle from closed to open state conformation.

conformation respectively and the average displacement at equilibrium agrees with the experimental observation. The tilt of channel S4 helix represents an opportunity to maintain the central pore conformation unaltered as well as the ion transportation [22]. In our study, this difference (17°–23°) from closed to open model (Fig. 2D) presumes that the upper portion of S4 (part of the paddle) is somewhat likely to find a position across the interfacial region of membrane, which is an important factor of paddle model of channel gating at activated conformation. As the tilt of S4 helix is not a property of helix screw model, it can be said that gating in Kv1.3 follow the idea of "paddle model" for channel gating like the other members of *Shaker*-type ion channel.

### 3.4. Validation of OSK1 and its derivatives

All the members of α-KTx3 toxin family share 68–90% sequence identity among each other [70]. An alignment of OSK1 along with the other members of α-KTx3 family is given in Fig. 3 showing their percentage of identity with OSK1 or α-KTx3.7. The OSK1 prevails some common differences among the other α-KTx3 toxins such as at position 16, instead of a lysine, an acidic glutamate residue is present (Fig. 3A). Similarly in position 20, OSK1 has a basic lysine residue where all other members contain an aspartic acid. And another distinctive feature of OSK1 is the presence of arginine at position 12 (while proline or glycine occurs in all other toxins). The works of Mouhat et al. revealed that, the order of *in-vivo* toxicity level in OSK1 decreases by introducing mutations at places like 12, 16, 20 or 25 [16]. In that case, OSK1-K16,D20 & OSK1-P12,K16,D20 are less toxic in comparison to OSK1 wild-type [16]. However, these alterations are believed to possess huge impacts on the peptide toxicity and their pharmacological effects. We also found very fair & distinctive conformations from our simulation studies.

The stability of OSK1 and its derivatives are assessed by DSSP profile, RMSD plots and RMS fluctuations (Fig. 4). It is evident from the DSSP plot that, OSK1 undergoes large structural modifications in mutated condition than its usual natural form (Fig. 4A). The α/β scaffold conformation of wild-type OSK1 is almost conserved during the whole simulation period. N-terminal 3–4 residues form a small beta sheet and has been described as a remarkable feature in OSK1, which merely adapts to an extended sheet conformation along with the amino acids Gly1–Lys9 [36,71]. Nevertheless, the presence of only two stranded beta sheet doesn't make the strand such disordered. In our study, the N-terminal beta sheet of OSK1 wild-type and OSK1-P12,K16,D20 further joins the other two anti parallel sheets and provide more stability to the whole β-sheet assembly. Similarly in case of OSK1-K16,D20 & OSK1-K16,D20,N25 mutants, the N-terminal end is highly excited and

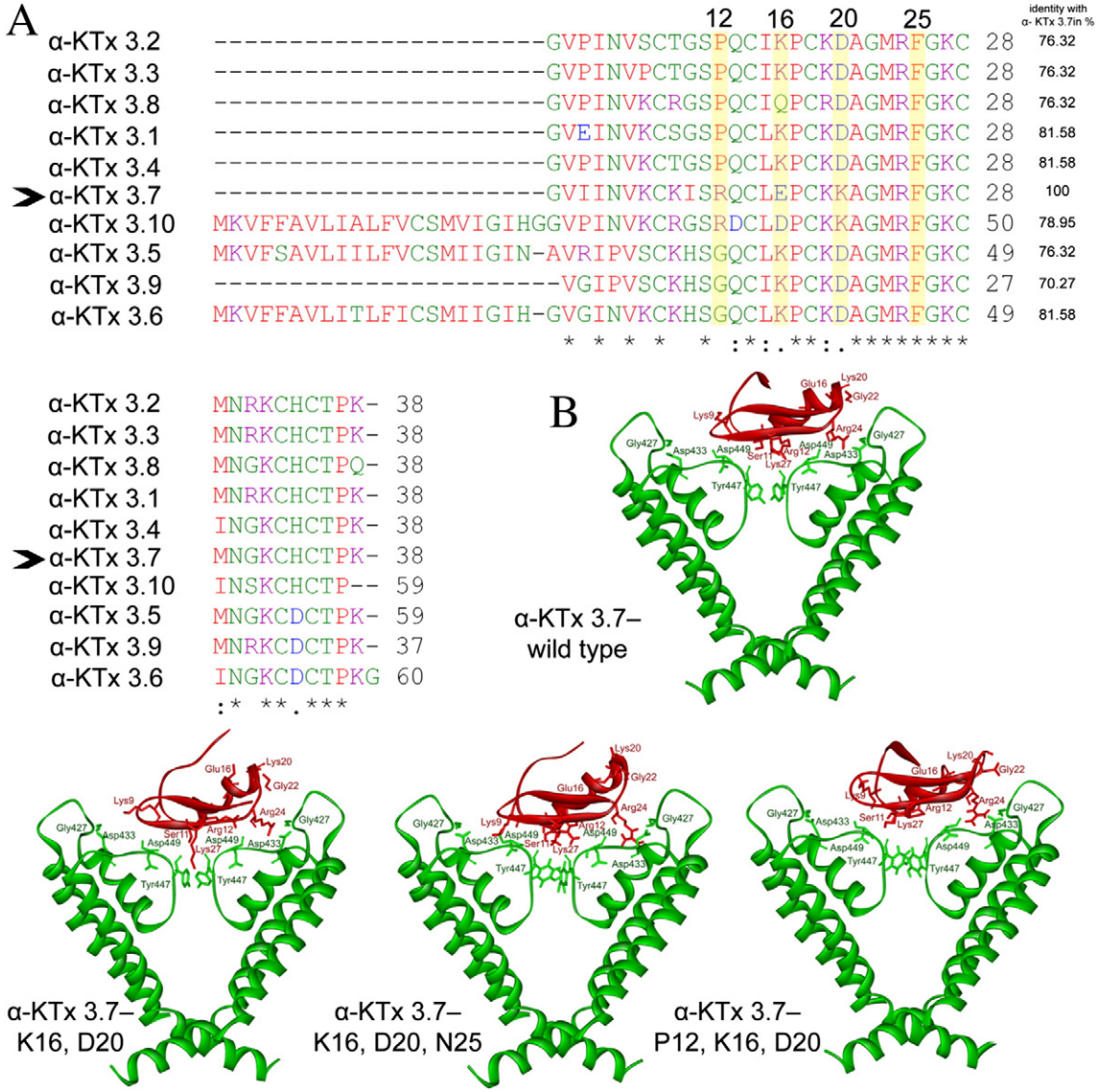


**Fig. 3.** (A) Sequence alignment of α-KTx3 family members and (B) channel–toxin docking complexes.

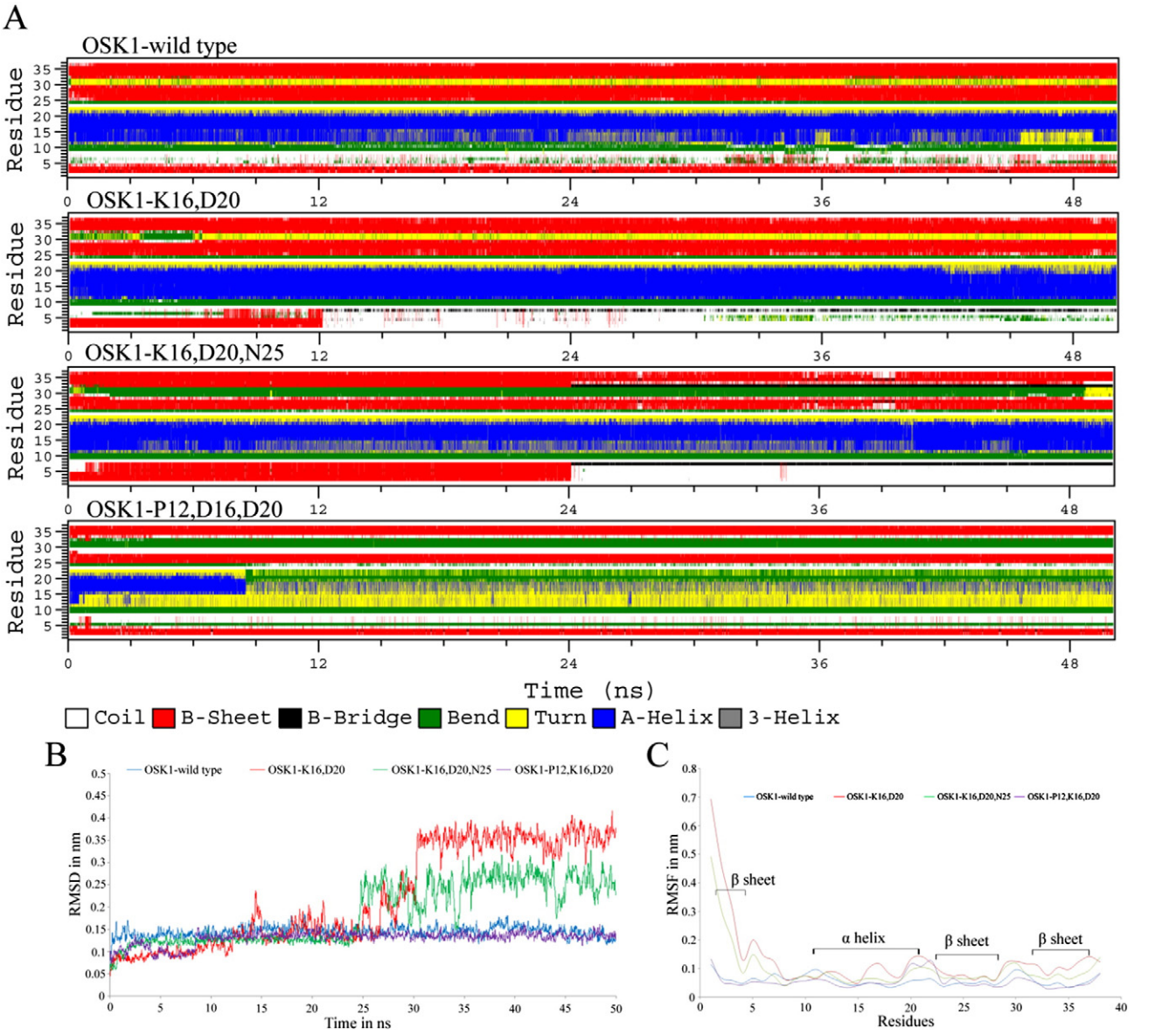


**Fig. 4.** (A) DSSP plots of OSK1 derivatives. (B) Comparison of toxin Cα atomic RMSD & (C) RMSF.

extended β-sheet conformation is detected for few ns and demolished further due to lack of enough hydrogen bonds before forming a three strand sheet. The opening beta strand of OSK1-K16,D20 disappears just after 12 ns of time, but presumes to have the most stable helix in comparison to all the system. Some new interesting features are observed, when the Asn25 mutation is associated along with OSK1-K16,D20 mutant. The length of initial beta strand extends from 3 to 8 amino acids and then completely replaced by a small beta bridge. In addition, a bend like conformation becomes more prominent between the last two sheets. Two other β-sheets (Met23–Met29 & Lys32–Lys38) contain mostly important inhibitory residues are comparatively more stable in all the four derivatives. The amphipathic helix (Ile10–Ala21) accommodates a proline at site 17, which has the ability to distort the α-helical structure by introducing a kink that results in bending the helix axis by 30° [36]. However, this property of all scorpion toxins is considered as an important feature for any biological role. The most striking configurational change is seen in OSK1-P12,K16,D20 mutated state, where insertion of a single proline in place of arginine helps to eliminate the helix and the overall pattern of stability is different from all other analogues.

These justifications are further supported by the RMDS & RMSF curves (Fig. 4B and C). The Cα RMSDs of all the OSK1 derivatives were bellow 2 Å till the first 25 ns of simulation followed by a sudden increase in OSK1-K16,D20 & OSK1-K16,D20,N25 mutated states, which are latter stabilized at a deviation of 3.5 Å & 2.5 Å respectively. Furthermore, OSK1 wild-type preserves the most stable conformation in every respect, further validated by Cα-RMSF graph. In comparison with the other mutant models, the OSK1-P12,K16,D20 shows less RMS deviation and moreover preserves its overall stability. The bond lengths of all three disulfide bridges are well maintained throughout the simulation in all OSK1 derivatives.

### *3.5. Characterization of Kv1.3 and OSK1 complexes by their stability, energetics and affinities*

The C-α RMSD of all the bound conformations are comparatively more stable than the Kv1.3 or OSK1 in free. Fig. S3 of Supplementary data shows that, the S4 segments and pore regions of Kv1.3 have attained the relative stability in all the Kv1.3–OSK1 complexes. In consistent with this expectation, we considered all the interacting residues

of their binding surfaces within 5 Å of contact. The toxins interact with the receptor by the pore as well as the typically unstructured loops at the outer vestibule regions above pore which contain abundantly negatively charged amino acids. The independent fluctuations of these interacting residues of Kv1.3 show comparatively less remarkable in complexes than the unbound conformations (Fig. S3). H-bonds and salt bridges also play effective role to their stability. From the salt bridge analysis, it's evident that, Lys7, Lys9, Arg12, Arg24 and Lys27 of OSK1 are able to form effective pair with the receptor residues Asp433, Asp449 or Asp272. Arginine at position 24 of all OSK1 derivatives is supposed to form salt bridges with Asp433 or Asp449 of Kv1.3 and these interactions are highly stable in the complexes with OSK1-K16,D20 & OSK1-P12,K16,D20 analogues [53]. But in case of OSK1 wild-type, these bridges lose their contacts after 30 ns of simulation and they are effectively weak in OSK1-K16,D20,N25. The side chain of the Arg12 in all OSK1 derivatives is fully extended, forms salt bridges with the acidic residues Asp433 and Asp449 in OSK1-K16,D20 only. The pore lining residue Asp449 of receptor actively participates in salt bridge interaction with the most conserved residue of α-KTx3 toxin family, Lys27 in OSK1-P12,K16,D20 throughout the simulation and with OSK1-K16,D20,N25 in last 15 ns of simulation. This salt bridge is completely absent in OSK1-K16,D20 and in OSK1 wild-type, it brings in an unstable one. Lys7–Asp272 creates a stable pair in OSK1-K16,D20,N25, which is absent in all other complexes. Lys9 comes closer to the pore residue Asp449 in OSK1 wild-type only. Even these particular residues are responsible to form H-bonds in the complexes. The average number of hydrogen bonds formed between receptor & toxin complexes are calculated as the summation of the number of H-bonds formed by complexes over the whole trajectories divided by the total number of frames (Table 1). The fractional values signify the formations and breaks of H-bond with time evolutions and it's apparent that, OSK1 wild-type forms more number of H-bonds with the receptor than all the mutant types. The compactness of the channel-toxin complex is further estimated by the interface accessible surface area differences.

The interface accessible surface area (ASA) denotes the surface area of the receptor and ligand involved in interaction indicating the protein–protein geometric fit/shape complementarity. A higher change in ASA always means of a better shape complementary between the molecules. ASA values between 1000 and 2000 $Å^2$ is a feature of stable enzyme–inhibitor complexes [72]. From our simulations we found that, OSK1-P12,K16,D20 owns the highest ΔASA value, which has a significant mode of binding with Kv1.3 channel. OSK1 wild-type and OSK1-K16,D20 comparatively report their complexes a bit less compact. Here we also note that the complexes are mainly characterized by the polar interfaces, suggesting the presence of H-bonds, which approve the non-obligatory nature of enzyme–inhibitor interactions. The ΔASA values from our result justify the harmony with the LIE binding free energy of our docked complexes.

A more quantitative characterization of the binding modes is provided by the average interaction energies added by the residues participated in interaction surface (Figs. 5 and 6). The Interaction Energy (IE) profile is the sum of van der Waals (VDW) and electrostatic (E) energy contribution of the individual residues located at the interface. In addition, the complexes with low interaction energies appear to be correlated with good interaction. Although all three toxin analogous bind tightly to the channel, OSK1-P12,K16,D20 seemed to be at the top on average interaction energy data (Table 1). For all four OSK1 analogues, the average electrostatic interaction energy is about 2–3 times higher than the VDW energy at the toxin bound state. The residues mostly involved either in hydrogen bonding or in hydrophobic interactions or in both are the principal contributors of exhibiting higher IE. Among the most interacting residues of OSK1, we noticed that lysine positioned at 27 protrudes into the channel pore during the toxin binding and consistently contribute a major portion of total interaction energy in all the four complexes. Similarly some other conserved amino acids such as Lys9, Arg12, Lys19, Arg24, Asn30 & LYS38, which directly participate in electrostatic or van-der-Waals interaction are affected in very dissimilar way due to mutagenesis (Fig. 5). From the receptor side, Asp449 is the principal IE contributor along with the Gly427, Asp433, Tyr447 and Gly448.

In OSK1 wild-type, the Lys27 interacts with carbonyl group of Tyr447 of the channel selectivity filter, independently contributed ~30% total interaction energy and makes extensive contacts with the channel pore equally by the whole tetrameric subunit. This deep penetration of Lys27 into the pore was consistent in two other mutants, OSK1-K16,D20 and OSK1-K16,D20,N25. The other residues such as Arg12 & Arg24 are supposed to be surrounded by Thr425, Ser426, Gly427 & Asp433 of two alternate outer vestibule units located just at outside the selectivity filter. In OSK1-K16,D20, these interactions provide some extra potential contacts to the binding interface. However, Arg12 of OSK1 wild-type remains close to the loop between S1 & S2 helices of channel (Thr269, Ser270 and Asp272) and offers less favorable electrostatic interaction in comparison to OSK1-K16,D20.

Residues Lys9 & Asn30 face same side of all toxin derivatives, allowing it to bind the channel selectivity filter more shallowly as well as the outer vestibule of the pore. But in OSK1-K16,D20 mutant, electrostatic interaction of these contacts are significantly weaker because of the upward movement of N-terminal part of toxin by losing its secondary structure. This issue is never found in the complexes having OSK1 wild-type or OSK1-P12,K16,D20 mutant. Similarly, the C-terminal end residue Lys38 is attracted by the negative amino acids like Glu420 and Asp433 of two opposite monomers of Kv1.3 having strong electrostatic interactions. This is noticed in all OSK1 analogues except the OSK1-K16,D20,N25.

Phe25 mainly take part in hydrophobic/VDW interaction in all OSK1 derivatives except the OSK1-K16,D20,N25. When a non-polar phenylalanine is substituted by an asparagine at position 25 along with K16,D20 mutation, it moves towards the channel pore with electrostatic interaction energy of −82.32 kJ/mol to the interaction surface. But the other important residues Lys9, Arg12 & Lys38 bend away from the channel wall. Consequently the overall interaction energy and the binding free energy of OSK1-K16,D20,N25 are found comparatively less effective, which gives a reason for this mutant significantly decreased potency of inhibition.

Most striking feature of interaction mechanism is observed in OSK1-P12,K16,D20 mutant, where a non-polar proline is introduced by replacing a charged residue arginine at position 12. Pharmacological surveys made by Mouhat et al. show that, this particular mutation along with K16,D20 should have a decreased activity towards all $K^+$ channels by 8- to 66-fold as compared with OSK1-K16,D20 and 4- to 36-fold as compared with OSK1 wild-type [39]. But, our finding went in contrary with this. The average channel–toxin interaction energy of

**Table 1**
Summary of channel–toxin interaction.

| Complex name | Average number of H-bonds with SD in the complex | ΔSASA of interaction surface in $Å^2$ | Average interaction energy between channel & toxin in kJ/mol | Binding free energy in kJ/mol |
|---|---|---|---|---|
| Kv1.3–OSK1 (wild type) | 11.15 ± 2.74 | 1217.67 | −773.91 ± 24 | −61.692 |
| Kv1.3–OSK1 (K16,D20) | 10.64 ± 2.23 | 1147.7 | −833.69 ± 28.2 | −44.332 |
| Kv1.3–OSK1 (K16,D20,N25) | 10.31 ± 2.45 | 790.57 | −594.65 ± 44 | −23.835 |
| Kv1.3–OSK1 (P12,K16,D20) | 10.73 ± 2.50 | 1231.33 | −879.62 ± 38.8 | −88.526 |

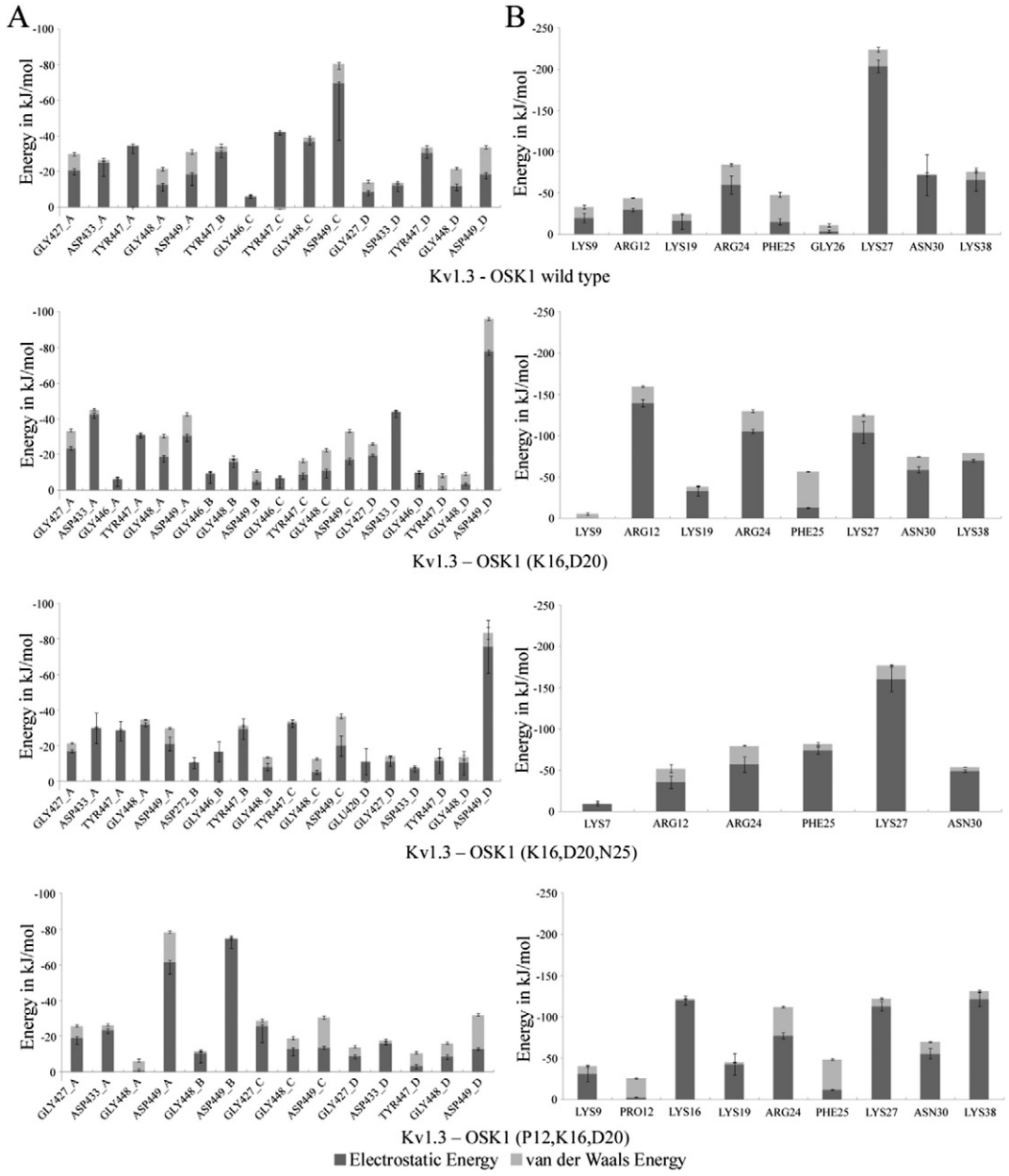


**Fig. 5.** Interaction energies contributed per residue in (A) Kv1.3 and (B) OSK1 derivatives.

OSK1-P12,K16,D20 comes on top of the chart. The mechanism of binding reveals that, the disruption of α helix by a proline allows the Lys16 to extend fully towards several residues like Ser273, Pro424, Ser426, Gly427, Ser429 & Asp433 establishing numerous H-bonds and electrostatic interaction. Here the Lys27 is less effective in providing electrostatic interaction in comparison to the other OSK1 derivatives and most of the interactions are stabilized by the surface contacts. Moreover, the other residues like Lys9, Arg24 & Asn30 participate in interaction more actively as they are identified in coil like conformation due to the increased space between the secondary structural elements in OSK1-P12,K16,D20.

In particular, we did not find have any direct effect of the mutagenic residues R12P, E16K, K20D or F25N on the large energetic variation on Kv1.3–OSK1 binding mode. As per the binding free energies can be correlated with the binding affinities, we have considered the LIE method to calculate free energies of these complexes (Table 1). It also signifies that the OSK1-P12,K16,D20 is more potent than all other OSK1 derivatives having lowest free energy value of −88.526 kJ/mol. However, the free energy of formerly justified OSK1-K16,D20 is less effective than the wild-type.

### 3.6. Potency and selectivity of OSK1 derivatives towards Kv1.3

In recent years, many attempts have been made to find more potent and highly selective toxin inhibitors to work against Kv1.3 by mutating their amino acid residues. Although no such pharmacological survey of those ligands has come out yet. So rather advocating for new mutational modifications, we analyzed the commonly instructed OSK1 derivatives interacting with Kv1.3 channel. In our study, the channel–toxin interactions helped to obstruct the displacement of channel S4 helix, prevent the ion conduction by OSK1 wild-type and all mutants. In previous studies it is reported that, both the potency and selectivity of these toxins towards Kv1.3 channel depends on the net positive charge from their amino acid composition and the positional conserved residues according to its family [39,73]. However, from the binding pattern of all OSK1 derivatives, it's clear that these mutations have drastically

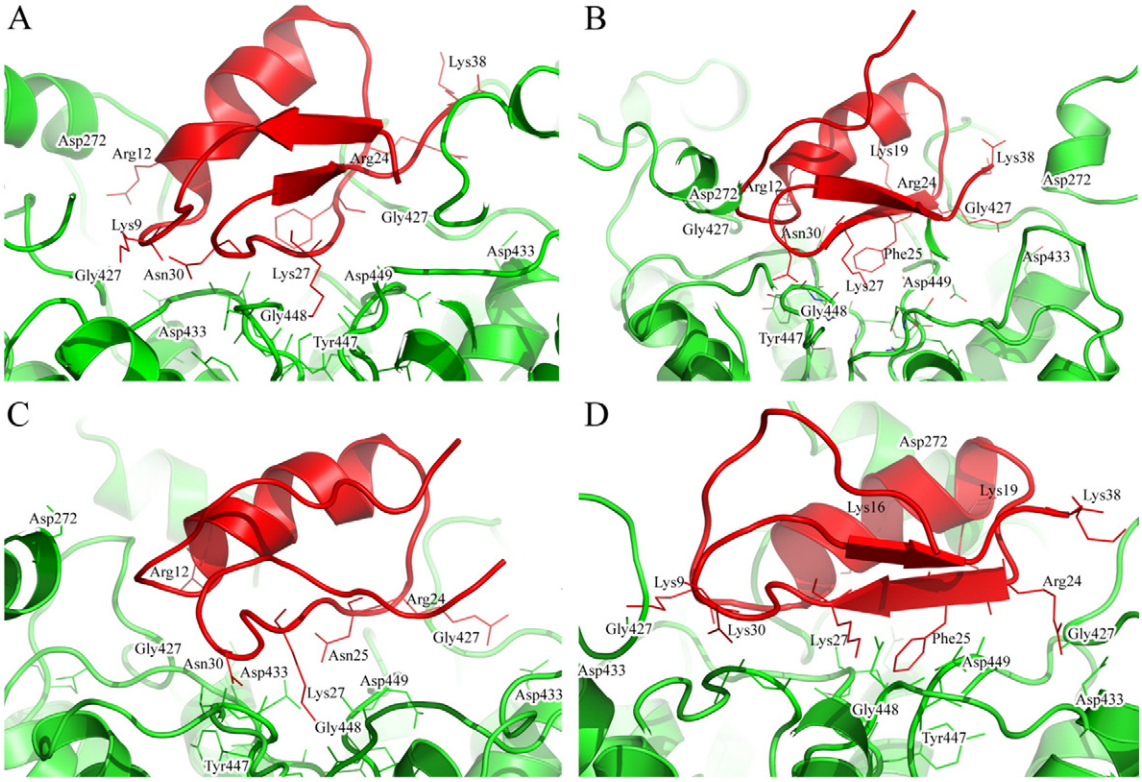


**Fig. 6.** Snapshots of binding surfaces of four complexes (A) OSK1 wild-type, (B) OSK1-K16,D20, (C) OSK1-K16,D20,N25 and (D) OSK1-P12,K16,D20.

influenced its potency. We also identified some key residues participating intensively in the interactions are present exclusively in Kv1.3 (Fig. S4 of Supplementary data). In particular, Asp272, Ser273, Pro424 & Gly427 of Kv1.3 channel are found to interact with the mutant toxin OSK1-K16,D20 and more specifically the OSK1-P12,K16,D20 in a signified manner, which justifies the increased sensitivity of Kv1.3 for the OSK1 mutant derivatives.

## 4. Conclusion

In this study, we have represented the dynamic activities of *Shaker*-type Kv1.3 ion channel in both open and closed state conformations embedded in DPPC bilayer as well as its interaction with OSK1 toxin analogues. Using computational approaches, we assessed their structural stabilities which report that, the channel in closed or inactivated form is comparatively more stable than its open active form. Being the part of *Shaker*-type "delayed rectifier" family of ion channels, Kv1.3 shows the rapidly inactivating property. This feature has been strengthened from our study, which also validates the reliability of our model. From the intra VSD salt bridge analysis, vertical drift of charged residues and lateral tilt of S4 helix, we found that the depolarization effect brought the upward displacement of S4 helix in open model in such as a way that agrees the idea of paddle model for the channel gating in Kv1.3.

The independent structural analysis of OSK1 derivatives revealed that, all the secondary structure assessments were conserved only in OSK1 wild-type, but the mutant derivatives went through large structural alterations. However, all these derivatives were able to form stable complexes with Kv1.3 channel. In the channel–toxin interaction sites, residues like Lys7, Lys9, Arg12, Arg24 and Lys27 were found to provide versatile interactions with the pore and surface lining residues of channel, where Lys27 firmly occluded the ion conduction path by forming strong electrostatic interaction. From the comparison of H-bond number, ΔASA and the energy terms among all the channel–toxin complexes, we identified two mutants OSK1-K16,D20 & OSK1-P12,K16,D20 possessing surplus increase in potency. Nevertheless, these amino acid alternations were not meant to affect the interaction directly. We also identified some specific residues of Kv1.3, which are responsible for toxin specificity over Kv1.1 & Kv1.2. We believe, more pharmacological survey on these OSK1 mutants is essential for their use as therapeutic drugs for several T-cell-mediated autoimmune diseases, since they are already declared as less toxic.

## Acknowledgments

The authors are thankful to Mr. Suman Kumar Nandy for his valuable suggestions and for reading the manuscript carefully. The whole study was supported by grants from BTIS net programme of DBT, Ministry of Science and Technology, Government of India, New Delhi and DST purse programme (BT/BI/25/001/2006).

## Appendix A. Supplementary data

Supplementary data to this article can be found online at http://dx.doi.org/10.1016/j.bpc.2015.04.004.

## References

[1] H. Wulff, H.G. Knaus, M. Pennington, K.G. Chandy, J. Immunol. 173 (2004) 776–786.
[2] R. Vicente, A. Escalada, M. Coma, G. Fuster, E. Sanchez-Tillo, C. Lopez-Iglesias, C. Soler, C. Solsona, A. Celada, A. Felipe, J. Biol. Chem. 278 (2003) 46307–46320.
[3] R. Khanna, L. Roy, X. Zhu, L.C. Schlichter, Am. J. Physiol. Cell Physiol. 280 (2001) C796–C806.
[4] S.A. Arkett, J. Dixon, J.N. Yang, D.D. Sakai, C. Minkin, S.M. Sims, Recept. Channels 2 (1994) 281–293.
[5] K. Schmidt, D. Eulitz, R.W. Veh, H. Kettenmann, F. Kirchhoff, Brain Res. 843 (1999) 145–160.
[6] D.A. Fadool, I.B. Levitan, J. Neurosci. 18 (1998) 6126–6137.
[7] F. Bezanilla, Physiol. Rev. 80 (2000) 555–592.
[8] F.J. Sigworth, Q. Rev. Biophys. 27 (1994) 1–40.
[9] S.A. Seoh, D. Sigg, D.M. Papazian, F. Bezanilla, Neuron 16 (1996) 1159–1167.
[10] S.K. Aggarwal, R. MacKinnon, Neuron 16 (1996) 1169–1177.
[11] F. Bezanilla, E. Perozo, E. Stefani, Biophys. J. 66 (1994) 1011–1021.
[12] W.N. Zagotta, T. Hoshi, R.W. Aldrich, J. Gen. Physiol. 103 (1994) 321–362.
[13] C.J. Smith-Maxwell, J.L. Ledwell, R.W. Aldrich, J. Gen. Physiol. 111 (1998) 399–420.

[14] M.O. Jensen, D.W. Borhani, K. Lindorff-Larsen, P. Maragakis, V. Jogini, M.P. Eastwood, R.O. Dror, D.E. Shaw, Proc. Natl. Acad. Sci. U. S. A. 107 (2010) 5833–5838.
[15] M.O. Jensen, V. Jogini, D.W. Borhani, A.E. Leffler, R.O. Dror, D.E. Shaw, Science 336 (2012) 229–233.
[16] S.B. Long, E.B. Campbell, R. Mackinnon, Science 309 (2005) 897–903.
[17] S.B. Long, X. Tao, E.B. Campbell, R. MacKinnon, Nature 450 (2007) 376–382.
[18] X. Tao, A. Lee, W. Limapichat, D.A. Dougherty, R. MacKinnon, Science 328 (2010) 67–73.
[19] X. Chen, Q. Wang, F. Ni, J. Ma, Proc. Natl. Acad. Sci. U. S. A. 107 (2010) 11352–11357.
[20] A. Banerjee, A. Lee, E. Campbell, R. Mackinnon, Elife 2 (2013) e00594.
[21] M.M. Pathak, V. Yarov-Yarovoy, G. Agarwal, B. Roux, P. Barth, S. Kohout, F. Tombola, E.Y. Isacoff, Neuron 56 (2007) 124–140.
[22] Y. Jiang, A. Lee, J. Chen, V. Ruta, M. Cadene, B.T. Chait, R. MacKinnon, Nature 423 (2003) 33–41.
[23] C.S. Gandhi, E. Loots, E.Y. Isacoff, Neuron 27 (2000) 585–595.
[24] S.Y. Lee, A. Banerjee, R. MacKinnon, PLoS Biol. 7 (2009) e47.
[25] M.D. Cahalan, K.G. Chandy, Immunol. Rev. 231 (2009) 59–87.
[26] S. Feske, E.Y. Skolnik, M. Prakriya, Nat. Rev. Immunol. 12 (2012) 532–547.
[27] C. Beeton, M.W. Pennington, H. Wulff, S. Singh, D. Nugent, G. Crossley, I. Khaytin, P.A. Calabresi, C.Y. Chen, G.A. Gutman, K.G. Chandy, Mol. Pharmacol. 67 (2005) 1369–1381.
[28] K.G. Chandy, H. Wulff, C. Beeton, M. Pennington, G.A. Gutman, M.D. Cahalan, Trends Pharmacol. Sci. 25 (2004) 280–289.
[29] H. Wulff, P.A. Calabresi, R. Allie, S. Yun, M. Pennington, C. Beeton, K.G. Chandy, J. Clin. Invest. 111 (2003) 1703–1713.
[30] P. Azam, A. Sankaranarayanan, D. Homerick, S. Griffey, H. Wulff, J. Investig. Dermatol. 127 (2007) 1419–1429.
[31] C. Beeton, J. Barbaria, P. Giraud, J. Devaux, A.M. Benoliel, M. Gola, J.M. Sabatier, D. Bernard, M. Crest, E. Beraud, J. Immunol. 166 (2001) 936–944.
[32] C. Beeton, H. Wulff, N.E. Standifer, P. Azam, K.M. Mullen, M.W. Pennington, A. Kolski-Andreaco, E. Wei, A. Grino, D.R. Counts, P.H. Wang, C.J. LeeHealey, S. A. B., A. Sankaranarayanan, D. Homerick, W.W. Roeck, J. Tehranzadeh, K.L. Stanhope, P. Zimin, P.J. Havel, S. Griffey, H.G. Knaus, G.T. Nepom, G.A. Gutman, P.A. Calabresi, K.G. Chandy, Proc. Natl. Acad. Sci. U. S. A. 103 (2006) 17414–17419.
[33] M.W. Pennington, C. Beeton, C.A. Galea, B.J. Smith, V. Chi, K.P. Monaghan, A. Garcia, S. Rangaraju, A. Giuffrida, D. Plank, G. Crossley, D. Nugent, I. Khaytin, Y. Lefievre, I. Peshenko, C. Dixon, S. Chauhan, A. Orzel, T. Inoue, X. Hu, R.V. Moore, R.S. Norton, K.G. Chandy, Mol. Pharmacol. 75 (2009) 762–773.
[34] E.J. Tarcha, V. Chi, E.J. Munoz-Elias, D. Bailey, L.M. Londono, S.K. Upadhyay, K. Norton, A. Banks, I. Tjong, H. Nguyen, X. Hu, G.W. Ruppert, S.E. Boley, R. Slauter, J. Sams, B. Knapp, D. Kentala, Z. Hansen, M.W. Pennington, C. Beeton, K.G. Chandy, S.P. Iadonato, J. Pharmacol. Exp. Ther. 342 (2012) 642–653.
[35] G. Panyi, L.D. Possani, R.C. Rodriguez de la Vega, R. Gaspar, Z. Varga, Curr. Pharm. Des. 12 (2006) 2199–2220.
[36] V.A. Jaravine, D.E. Nolde, M.J. Reibarkh, Y.V. Korolkova, S.A. Kozlov, K.A. Pluzhnikov, E.V. Grishin, A.S. Arseniev, Biochemistry 36 (1997) 1223–1232.
[37] S. Mouhat, B. Jouirou, A. Mosbah, M. De Waard, J.M. Sabatier, Biochem. J. 378 (2004) 717–726.
[38] E.V. Grishin, Yu.V. Korolkova, S.A. Kozlov, A.V. Lipkin, E.D. Nosyreva, K.A. Pluzhnikov, S.V. Sukhanov, T.M. Volkova, Pure Appl. Chem. 68 (1996) 2105–2109.
[39] S. Mouhat, V. Visan, S. Ananthakrishnan, H. Wulff, N. Andreotti, S. Grissmer, H. Darbon, M. De Waard, J.M. Sabatier, Biochem. J. 385 (2005) 95–104.
[40] M.A. Larkin, G. Blackshields, N.P. Brown, R. Chenna, P.A. McGettigan, H. McWilliam, F. Valentin, I.M. Wallace, A. Wilm, R. Lopez, J.D. Thompson, T.J. Gibson, D.G. Higgins, Bioinformatics 23 (2007) 2947–2948.
[41] N. Eswar, D. Eramian, B. Webb, M.Y. Shen, A. Sali, Methods Mol. Biol. 426 (2008) 145–159.
[42] S. Pronk, S. Pall, R. Schulz, P. Larsson, P. Bjelkmar, R. Apostolov, M.R. Shirts, J.C. Smith, P.M. Kasson, D. van der Spoel, B. Hess, E. Lindahl, Bioinformatics 29 (2013) 845–854.
[43] W. Kabsch, C. Sander, Biopolymers 22 (1983) 2577–2637.
[44] The PyMOL Molecular Graphics System, Version 1.1, 2002. Schrödinger, LLC.
[45] R. Bhuyan, A. Seal, J. Membr. Biol. (2014) 1–15, http://dx.doi.org/10.1007/s00232-014-9764-7.
[46] A.D. MacKerell, D. Bashford, M. Bellott, R.L. Dunbrack, J.D. Evanseck, M.J. Field, S. Fischer, J. Gao, H. Guo, S. Ha, D. Joseph-McCarthy, L. Kuchnir, K. Kuczera, F.T. Lau, C. Mattos, S. Michnick, T. Ngo, D.T. Nguyen, B. Prodhom, W.E. Reiher, B. Roux, M. Schlenkrich, J.C. Smith, R. Stote, J. Straub, M. Watanabe, J. Wiorkiewicz-Kuczera, D. Yin, M. Karplus, J. Phys. Chem. B 102 (1998) 3586–3616.
[47] H.J.C. Berendsen, J.R. Grigera, T.P. Straatsma, J. Phys. Chem. 91 (1987) 6269–6271.
[48] G. Bussi, D. Donadio, M. Parrinello, J. Chem. Phys. 126 (2007) 014101.
[49] M. Parrinello, A. Rahman, J. Appl. Phys. 52 (1981) 7182–7190.
[50] T. Darden, D. York, L. Pedersen, J. Chem. Phys. 98 (1993) 10089–10092.
[51] B. Hess, H. Bekker, H.J. Berendsen, J.G. Fraaije, J. Comput. Chem. 18 (1997) 1463–1472.
[52] R. Chen, L. Li, Z. Weng, Proteins 52 (2003) 80–87.
[53] C.S. Park, C. Miller, Neuron 9 (1992) 307–313.
[54] L. Yu, C. Sun, D. Song, J. Shen, N. Xu, A. Gunasekera, P.J. Hajduk, E.T. Olejniczak, Biochemistry 44 (2005) 15834–15841.
[55] J. Aqvist, C. Medina, J.E. Samuelsson, Protein Eng. 7 (1994) 385–391.
[56] J. Aqvist, V.B. Luzhkov, B.O. Brandsdal, Acc. Chem. Res. 35 (2002) 358–365.
[57] H. Wang, D.D. Kunkel, P.A. Schwartzkroin, B.L. Tempel, J. Neurosci. 14 (1994) 4588–4599.
[58] W.A. Coetzee, Y. Amarillo, J. Chiu, A. Chow, D. Lau, T. McCormack, H. Moreno, M.S. Nadal, A. Ozaita, D. Pountney, M. Saganich, E. Vega-Saenz de Miera, B. Rudy, Molecular diversity of K+ channels, Ann. N. Y. Acad. Sci. 868 (1999) 233–285.
[59] J. Zhu, I. Watanabe, A. Poholek, M. Koss, B. Gomez, C. Yan, E. Recio-Pinto, W.B. Thornhill, Biochem. J. 375 (2003) 769–775.
[60] L.W. Tu, C. Deutsch, J. Mol. Biol. 396 (2010) 1346–1360.
[61] P. Bjelkmar, P.S. Niemela, I. Vattulainen, E. Lindahl, PLoS Comput. Biol. 5 (2009) e1000289.
[62] F. Khalili-Araghi, V. Jogini, V. Yarov-Yarovoy, E. Tajkhorshid, B. Roux, K. Schulten, Biophys. J. 98 (2010) 2189–2198.
[63] C.A. Villalba-Galea, W. Sandtner, D.M. Starace, F. Bezanilla, Proc. Natl. Acad. Sci. U. S. A. 105 (2008) 17600–17607.
[64] G.M. Clayton, S. Altieri, L. Heginbotham, V.M. Unger, J.H. Morais-Cabral, Proc. Natl. Acad. Sci. U. S. A. 105 (2008) 1511–1515.
[65] F. Tombola, M.M. Pathak, E.Y. Isacoff, Neuron 45 (2005) 379–388.
[66] H.R. Guy, P. Seetharamulu, Proc. Natl. Acad. Sci. U. S. A. 83 (1986) 508–512.
[67] W.A. Catterall, Science 242 (1988) 50–61.
[68] B. Chanda, O.K. Asamoah, R. Blunck, B. Roux, F. Bezanilla, Nature 436 (2005) 852–856.
[69] V. Ruta, J. Chen, R. MacKinnon, Cell 123 (2005) 463–475.
[70] J. Tytgat, K.G. Chandy, M.L. Garcia, G.A. Gutman, M.F. Martin-Eauclaire, J.J. van der Walt, L.D. Possani, Trends Pharmacol. Sci. 20 (1999) 444–447.
[71] H. Darbon, E. Blanc, J.M. Sabatier, Perspect. Drug Discov. 15 (1999) 41–60.
[72] I.M. Nooren, J.M. Thornton, EMBO J. 22 (2003) 3486–3492.
[73] G. Corzo, F. Papp, Z. Varga, O. Barraza, P.G. Espino-Solis, R.C. Rodriguez de la Vega, R. Gaspar, G. Panyi, L.D. Possani, Biochem. Pharmacol. 76 (2008) 1142–1154.